Preparation of TiO₂/activated carbon with Fe ions doping photocatalyst and its application to photocatalytic degradation of reactive brilliant red K2G

LI YouJi[†], LI Jing, MA MingYuan, OUYANG YuZhu & YAN WenBin

College of Chemistry and Chemical Engineering, Jishou University, Jishou 416000, China

Titanium dioxide coated on activated carbon (AC) with Fe ions doping (Fe-TiO₂/AC) composite was prepared by an improved sol-gel method. The photocatalytic activities were tested by photocatalytic degradation of reactive brilliant red K2G in solution. The results show that in comparison with the agglomeration of pure TiO₂, the TiO₂ nanoparticles are well dispersed in the AC matrix, of which sizes are decreased with Fe ions doping. Additionally, the iron species on TiO₂ of composite are Fe₂O₃ and FeO, which do not affect the crystalline structures of TiO₂ nanoparticles. The AC matrix and iron doping content influence the fluorescence intensity of composite due to their effects on recombination probability of hole-electron pairs. Compared with TiO₂, 0.3% Fe-TiO₂, TiO₂/AC, 0.5% Fe-TiO₂/AC and 0.1% Fe-TiO₂/AC, the 0.3% Fe-TiO₂/AC shows the highest photoactivity with the complete mineralization of K2G for finite time due to the optimum Fe ions content and AC matrix. Furthermore, the kinetic constant ($k = 0.0229$ min⁻¹) of 0.3% Fe-TiO₂/AC composite is more than the sum of both TiO₂/AC (0.0154 min⁻¹) and 0.3% Fe-TiO₂ (0.0057 min⁻¹) because coexistence of the AC and Fe ions has an enlarging effect on improving the photoactivity of TiO₂.

TiO₂ nanoparticles, Fe ions, activated carbon, photocatalysis, reactive brilliant red K2G

1 Introduction

Industrialization and agricultural development, together with a rapid growth of human population, have all contributed to the drastic reduction in the number of available clean water resources. With the growing awareness of this worrying decrease in available water resources, many methods, including physical, chemical, and biological methods, are being used in wastewater treatment and recycling. Among them, heterogeneous photocatalysis appears to be an emerging technology leading to the total mineralization of most organic pollutants[1−6]. TiO₂ is the most widely used photocatalyst because of its excellent photoactivity, chemical stability, commercial availability, and low cost. However, because the fine TiO₂ particles are commonly of nanometer size proportions, the problem of separation and recovery of this

photocatalyst from the reaction medium is a major concern. An alternative method involves the immobilization of TiO₂ powder on an inert and suitable supporting matrix[7−13]. Due to its good adsorption properties, activated carbon (AC) is widely used as a matrix in gas and water remediation, and its use in the matrix of TiO₂ exhibits a synergism that has marked effects on the kinetics for removing pollutants, where each pollutant is more rapidly photodegraded[14−16]. Recombination of generated e⁻/h⁺ pairs affects the amount of active oxygen species produced by charge trapping. To suppress annihilation of the photogenerated e⁻/h⁺ pairs, studies of

selective metal ion doping of the crystalline TiO_2 matrix have been carried out; this is the most popular technique for modification of the TiO_2 surface[17,18]. However, the effect of metal ion doping strongly depends on many factors such as the dopant concentration, the particle size of the nanocrystalline TiO_2, the distribution of the dopants and the d-electronic configuration of doping ions[19]. The radii of Fe^{3+} and Ti^{4+} are 0.69 and 0.74 Å, respectively. According to Pauling's principle, it is easy for Fe^{3+} ion to cooperate with the matrix of the TiO_2 nanoparticles without causing much crystalline distortion[20].

It has been known that the right adulteration and load are beneficial to improving the photocatalytic activities of TiO_2. However, there have been only a few studies on TiO_2 nanoparticles coated on activated carbon (AC) with metal ions doping. Here, AC and Fe ions were respectively selected as an adsorptive matrix and dopant to prepare TiO_2 composite. Reactive brilliant red K2G was chosen as the model pollutant to evaluate the photocatalytic efficiency of the obtained catalysts

2 Experimental

2.1 Sample preparation

Tetrabutyl orthotitanate, diethanolamine, $Fe(NO_3)_3$ and ethanol were analytically pure. The doubly-distilled water was prepared in self-experiment. Activated carbon grains (average particle size: 0.12 cm, surface area: 482.9 m^2/g, total pore volume: 0.3640 $cm^3 \cdot g^{-1}$) were prepared by the vapor activation of coconut shell. To prepare iron-modified photocatalysts, known amounts of $Fe(NO_3)_3$ solution were added during the preparation of the TiO_2 sol. The particular preparation by an improved sol-gel method is followed: The appropriate amount of $Fe(NO_3)_3$ was dissolved in doubly-distilled water containing muriatic acid prior to hydrolysis of $Ti(OC_4H_9)_4$. Tetrabutyl orthotitanate (17.0 mL) and diethanolamine were dissolved in ethanol. The solution was stirred vigorously at 20℃, followed by the addition of a mixture of doubly-distilled water containing $Fe(NO_3)_3$ and ethanol. The resulting alkoxide solution was left at 20℃ to hydrolyze to a Fe-TiO_2 sol. Then a desired amount of activated carbon grains was immersed into the Fe-TiO_2 sol with a certain viscosity, and the mixture stirred in an ultrasonic bath. When the Fe-TiO_2 sol coated on the sealing substrates changed to a Fe-TiO_2 gel, the substrates were vacuum-dried by subsequently repeating the process

from immersing to dryness. Finally, the grains obtained were first heat-treated at 250℃ for 2 h in air and then at 500℃ in nitrogen for 2 h to prepare n%Fe-TiO_2/AC. Here n means Fe content in TiO_2. Additional naked Fe-TiO_2 powders and undoped TiO_2/AC were prepared as a reference using the same hydrolysis procedure for tetrabutyl orthotitanate. In analyzing course of FS spectra, TiO_2 + AC and 0.3%Fe-TiO_2 + AC mean the TiO_2 and 0.3%Fe-TiO_2 are simply mixed with AC, respectively.

2.2 Characterization

The obtained Fe–TiO_2/AC composite was detected by measuring their respective BET surface areas using the nitrogen absorption method (ASAP2010, Micromeritics Company, USA) at 77 K. The crystalline phase was identified by X–ray diffraction (Bruker, Germany) using Cu-Kα as radiation. The morphology of the prepared catalysts was observed by SEM (JSM-5600LV, Japan). The chemical state of titanium, oxygen and iron on the surface and near surface of the deposited active carbon was studied by X-ray photoelectron spectroscopy, using a VG Scientific ESCALAB Mark Spectrometer (England), where MgKα radiation was used (1253.6 eV). The X-ray photoelectron spectra were reference to the C1s peak (Eb = 285.0 eV). The fluorescence spectra of catalysts were measured by a Jasco FP-777 Fluorescence Spectrophotometer at an excitation wavelength of 320 nm. Fe content in TiO_2 was calculated by high resolution inductively coupled plasma mass spectrometry (HR-ICP-MS, Micromass, England). The amount of TiO_2 doped on the carbon surface was estimated from ignition loss at 800℃ in air by using TG apparatus (Netzsch, Germany).

2.3 Photocatalytic degradation of reactive brilliant red K2G

Reactive brilliant red K2G was chosen as a model organic compound to evaluate the photoactivity of the prepared samples. Figure 1 shows a scheme of the experimental equipment (volume 280 mL). The main component of the system was the reactor, accompanied with internal stirring by air sparging with a flow capacity of 56 mL/s. A 60 W ultraviolet lamp was positioned inside a pyrex cell, and the wavelength range and peak wavelength of the UV lamp were 320−400 nm and 365 nm, respectively. Photocatalyst (0.5 g) was suspended in 200 mL air-sparged aqueous solution containing reactive brilliant red K2G (20 mg·L^{-1}) in the above
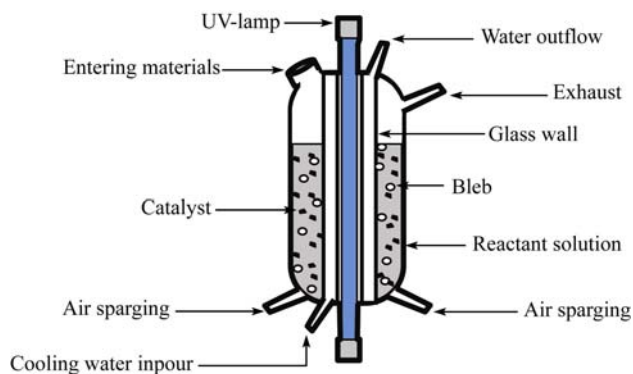
Figure 1 Experimental equipment for the photocatalytic reaction.

pyrex reaction vessel. The temperature of photocatalytic reaction was maintained at 25℃ by water circulation. To determine the change in K2G concentration in solution during the process, a solution of a few milliliters was taken from the reaction mixture, subsequently centrifuged, and filtered through a Millipore filter (pore size 0.22 μm) to separate the catalysts, and loaded in a UV-Vis spectrometer (JascoV-500, Japan). The K2G concentration was calculated from the absorbance at 509 nm using a calibration curve. The extent of mineralisation was determined using a total organic carbon (TOC) analyser (Euroglas TOC 1200).

3 Results and discussion

Nitrogen adsorption isotherms and pore size distributions for AC and 0.3 % Fe-TiO$_2$/AC are shown in Figure 2. The surface area of AC mainly in the mesopore range was determined to be 483.2 m^2/g. For the 0.3% Fe-TiO$_2$/AC sample, the surface area decreased to 470.6 m^2/g. The inclusion of 0.3% Fe-TiO$_2$ nanoparticles with low
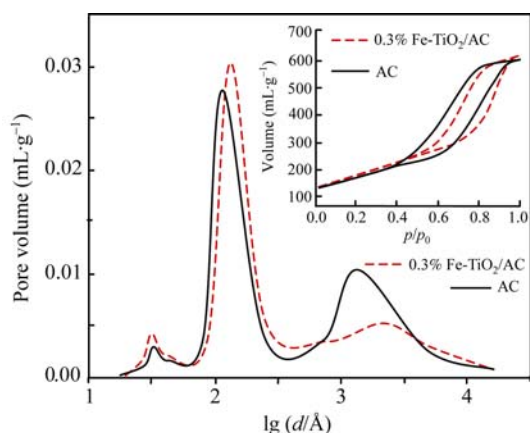

Figure 2 Pore size distributions of original AC, and 0.3% Fe-TiO$_2$/AC. Inset: N$_2$ adsorption isotherms of original AC and 0.3% Fe-TiO$_2$/AC.

surface areas was responsible for the decline in surface area. From the corresponding pore size distribution curves, it can be seen that there was little change in the mesopore size distribution of the 0.3% Fe-TiO$_2$/AC sample. This result indicates that the AC matrix maintained a relatively high surface area with the same pore structure after loading with 0.3% Fe-TiO$_2$. As indicated in Figure 3, the macropores and mesopores of AC are not blocked by the TiO$_2$ nanoparticles with 0.3% Fe doping, and this is why 0.3% Fe-TiO$_2$/AC composite has high surface areas. To study multistructure of Fe-TiO$_2$ nanoparticles on the AC surface, the selected region is magnified as shown in Figure 3(b). The white particles on the composite surface are sphere-like TiO$_2$ particles with Fe doping, while the multi-pore faces are amorphous AC in nature, and individual crystalline particles and the AC matrix are clearly distinguished from the SEM micrographs. Compared to agglomeration of pure TiO$_2$ (Figure 3(d)), the sphere-like particles are well dispersed in the AC matrix due to cumbering effect of AC on the TiO$_2$ particles reuniting as shown in Figure 3(b) and (c). Additionally, particle sizes of 0.3% Fe-TiO$_2$/AC, TiO$_2$/AC and pure TiO$_2$ are evidently observed to have the following sequence: 0.3%Fe-TiO$_2$/AC (about 20 nm) < TiO$_2$/AC (about 30 nm)< pure TiO$_2$ (about 50 nm). It is attributed to the fact that Fe ions also act as barriers that control the growth of the TiO$_2$ particles to a certain extent besides baffling effects of AC matrix on growth of the TiO$_2$ particles. The XRD patterns of 0.3% Fe-TiO$_2$/AC annealed at 500℃ for 2 h are shown in Figure 4. The XRD peak of crystal plane 101 for anatase appeared at 25.4° (2θ) and crystal plane 110 for rutile appeared at 27.5° (2θ), which is in agreement with the literature[21], and additionally, graphite is attributed to amorphous phases of activated carbon. No Fe peak was observed on 0.3% Fe-TiO$_2$/AC, perhaps due to the microscale of Fe ions and similar radii of iron and titanium. It is indicated that the Fe ions did not affect the crystalline structures of the TiO$_2$-coated AC. The average crystalline sizes of all sol-gel-derived TiO$_2$ are nearly 18 nm, calculated from the Scherrer's equation, which are consistent with the SEM observation displayed in Figure 3(b).

Figure 5 displays the XPS spectra of 0.3% Fe-TiO$_2$/AC, and irrespective of the growth parameters, and only lines characteristics of titanium, oxygen and carbon can be observed with a small protuberance of iron element.
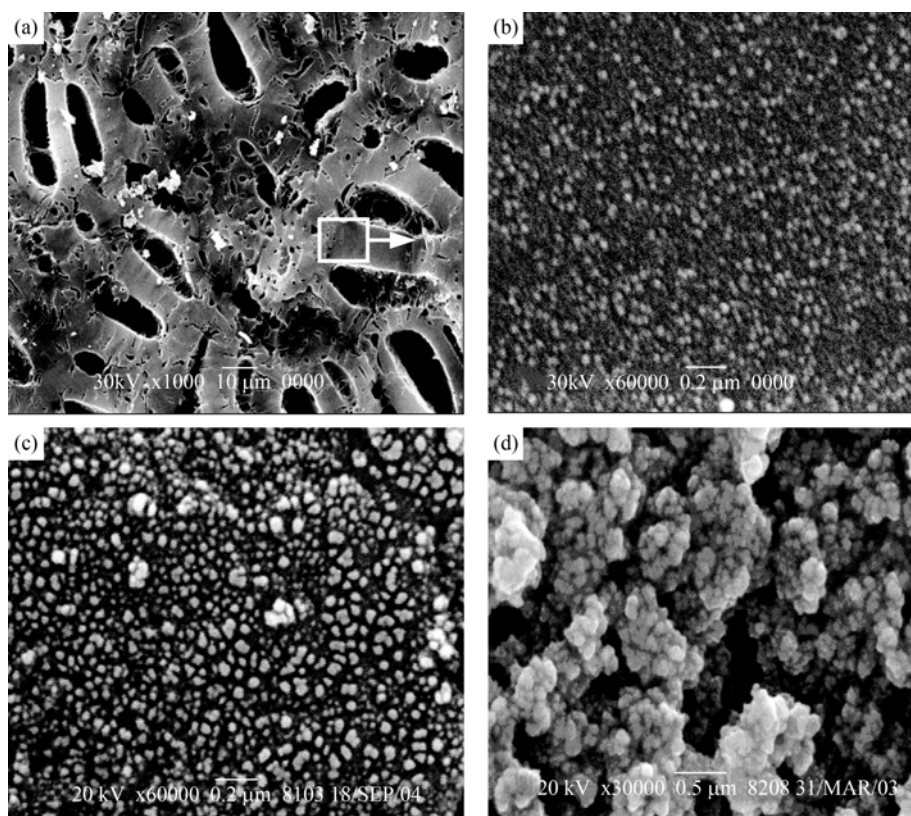
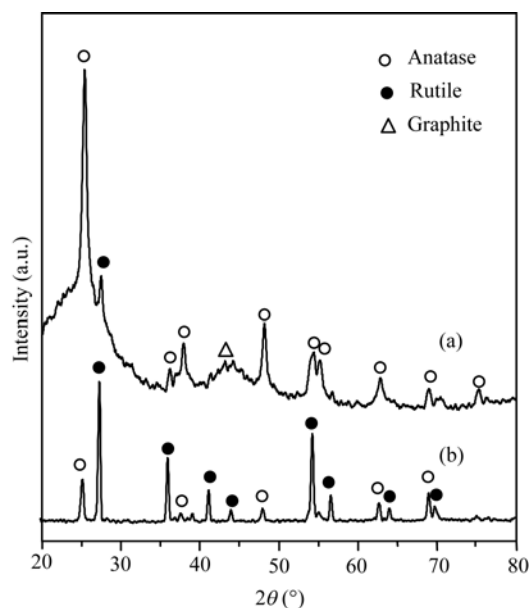**Figure 3** SEM images of samples. (a) and (b) 0.3% Fe-TiO₂/AC; (c) TiO₂/AC; (d) pure TiO₂.
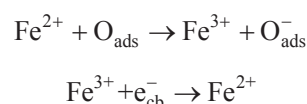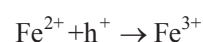

Figure 4 XRD patterns of 0.3% Fe-TiO₂/AC (a) and pure TiO₂ (b) annealed at 500℃ for 2 h.

The binding energy of Ti2p$_{3/2}$ and 2p$_{1/2}$ is the same as that of pure titania at 459.4 and 465.3 eV, respectively, indicating the integrity of the TiO₂ structure, which has not been modified by iron doping. It can be seen from the XPS curve fitting of the Fe2p XPS peak in Figure 5(b) that the two peaks correspond to two kinds of Fe species on the sample surface. The binding energy of 709.2 eV is the characteristic for FeO, while the higher binding energy of 710.6 eV is the characteristic for Fe₂O₃. It is supposed that the coexistence of Fe^{3+} and Fe^{2+} can improve the photocatalytic efficiency according to the following:

$$Fe^{2+} + O_{ads} \rightarrow Fe^{3+} + O_{ads}^-$$

$$Fe^{3+} + e_{cb}^- \rightarrow Fe^{2+}$$

On the one hand, the Fe^{3+} ions can trap the excited electrons in the conduction band, thus inhibiting the electron/hole pair recombination; on the other hand, the Fe^{2+} ions can supply an electron to the oxygen adsorbed on the surface of the catalyst, thus accelerating the interfacial electron transfer[22]. However, decreased activity above the optimum metal ions concentration is possibly due to the oxidation of Fe^{2+} ions by hydroxyl radicals or holes:

$$Fe^{2+} + h^+ \rightarrow Fe^{3+}$$

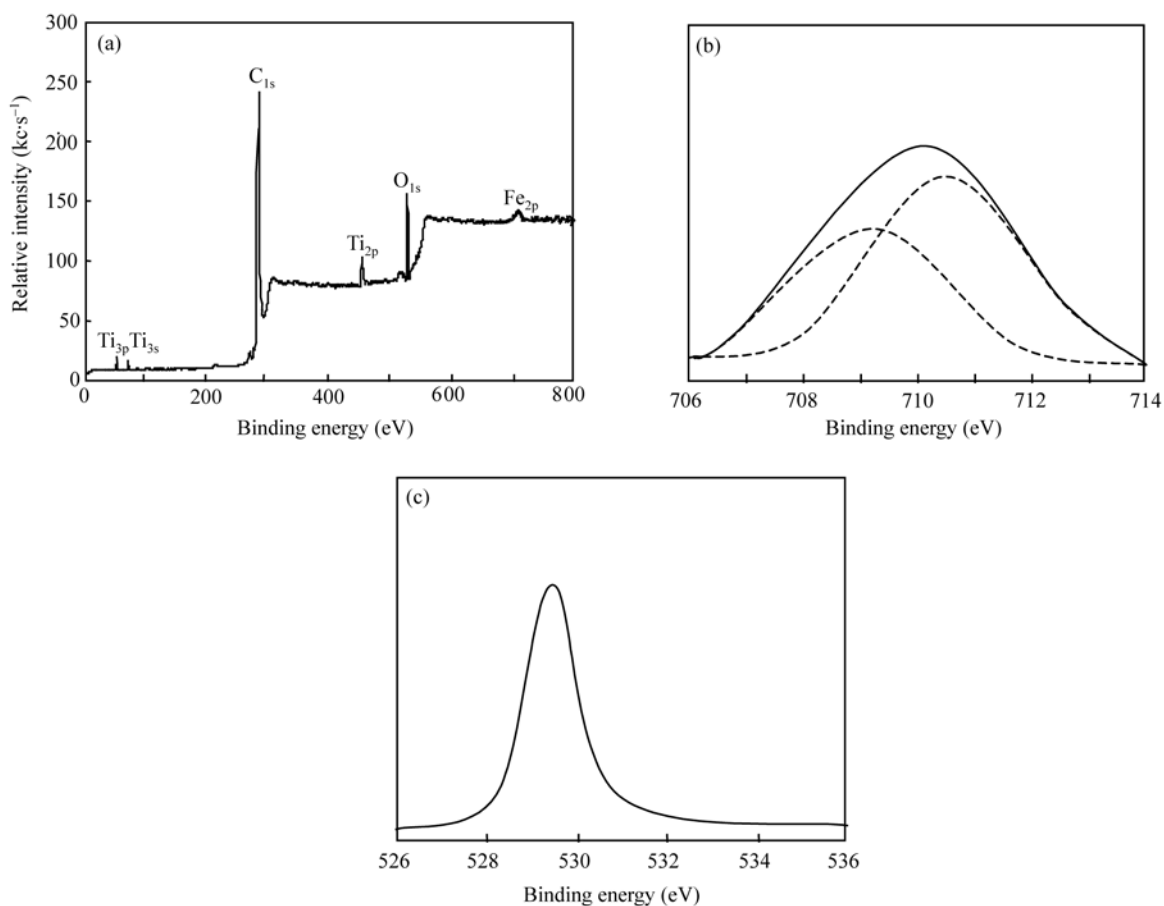So the optimized content of iron doping is essential

Figure 5 XPS spectra of 0.3% Fe-TiO$_2$/AC (a), the curve-fitting of the Fe2p XPS (b) and the curve-fitting of the O1s XPS (c).

for the high photoactivity of composite. Figure 5(c) illustrates the high resolution XPS spectra of the O1s region for the surface of 0.3% Fe-TiO$_2$/AC. The binding energy of O1s is 529.7 eV, which can be assigned to the O1s in the TiO$_2$ lattice. Additionally, it is evidently observed that the binding energy can not be decomposed into 531.95 eV, which is equal to that of O atom in hydroxyl[23]. It is also suggested that there are Fe^{2+} ions probably existing on catalysts surface. The surface functionalization of samples was further proven by fluorescence spectroscopy, as illustrated in Figure 6. In order to avoid the effect of TiO$_2$ content on fluorescence intensity, all samples with AC content of about 85% were dissolved in vacuum for measurement of their emission spectra exciting at 250 nm. Clearly, different intensity of fluorescence spectra nearly around 470 nm is related with Fe doping content and AC. The fluorescence of titania is caused by the recombination of electrons and holes[24]. The decline in fluorescence intensity is due to the reduced number of recombination sites on the TiO$_2$ surface. Fewer recombination sites on the surface lead to

slower recombination of electrons and holes, which means higher separation ratio of electrons and holes, and a higher photocatalytic activity[25]. Compared with pure TiO$_2$ and 0.5% Fe-TiO$_2$, the fluorescence intensity of TiO$_2$/AC and 0.5% Fe-TiO$_2$/AC is low, respectively, in
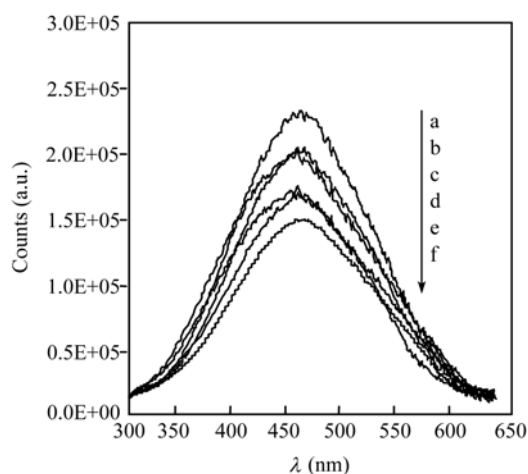

Figure 6 FS spectra of different samples (λ_{ex} = 250 nm). a, TiO$_2$ + AC; b, 0.3% Fe-TiO$_2$ + AC; c, TiO$_2$/AC; d, 0.1% Fe-TiO$_2$/AC; e, 0.5% Fe-TiO$_2$/AC; f, 0.3% Fe-TiO$_2$/AC. AC constant is about 85% in all samples.

that carbon substrate also reduces TiO_2 to form more Ti^{3+} ions besides residual carbon in the nanoparticles from organic radicals. By acting as an active center, Ti^{3+} can trap the photogenerated electrons in the conduction band and prevent the recombination of electron-hole pairs under UV. Due to both effects of the optimum iron ions content and AC matrix, the 0.3% $Fe-TiO_2/AC$ effectively provides the most electron traps and gives the lowest fluorescence intensity.

As shown in Figure 7, adsorption of AC reaches saturation point after 200 min, while 0.3% $Fe-TiO_2/AC$ shows zero decomposition after 200 min without UV irradiation. It is considered that the decomposition of K2G mainly occurred on the $Fe-TiO_2$ particles. As such, the decomposition of K2G must be related to the structure of the catalysts. By comparison, the relation between the K2G photodegradation rate and the catalysts follows the sequence: 0.3% $Fe-TiO_2/AC$>0.5% $Fe-TiO_2/AC$>0.1% $Fe-TiO_2/AC$>TiO_2/AC>0.3% $Fe-TiO_2$>P25>TiO_2. The obtained results are consistent with the fluorescence intensity. Additionally, TOC results reveal that under optimal conditions, pure TiO_2 and TiO_2/AC require 550 min and 420 min for complete mineralisation of K2G, however 0.3% $Fe-TiO_2/AC$ requires only 310 min, which shows the higher relative photocatalytic efficiency for both degradation and mineralisation, because the use of Fe ions as dopant agent plays a role in improving the photoinduced charge separation in the nanostructured semiconductor and in the interfacial charge tra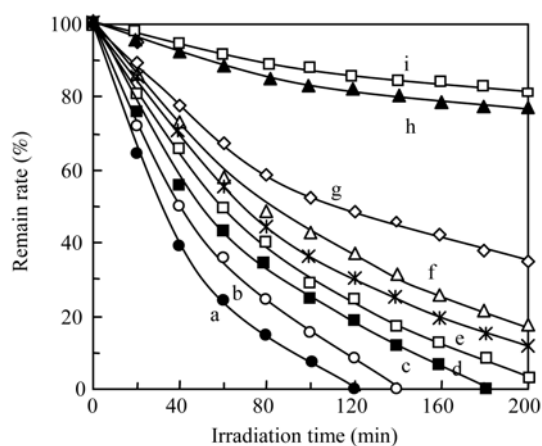nsfer process at the semiconductor/solution interface, and activated carbon produces a high concentration of K2G near the $Fe-TiO_2$ photocatalysts to be decomposed. Additionally, it was found that photocatalytic degradation of K2G was fit for the first-order equation by these catalysts in previous studies. The kinetic constant ($k = 0.0229$ min^{-1}) of 0.3% $Fe-TiO_2/AC$ composite is more than the sum of both TiO_2/AC (0.0154 min^{-1}) and 0.3% $Fe-TiO_2$ (0.0057 min^{-1}). This result seems to indicate that coexistence of the AC and Fe ions has an enlarging effect on improving the photoactivity of TiO_2, which is greater than the effect of AC or Fe ions alone. The photodegradation efficiency of TiO_2 depends on the illuminated catalyst surface area in contact with the solution and on the mass transfer to the catalyst surface[10]. For the $Fe-TiO_2/AC$ composite, the process of removal of K2G molecules can be schematically illustrated, as shown in Figure 8. Due to the strong adsorption ability of AC, the K2G molecules concentrated around the $Fe-TiO_2/AC$ composite increase the probability of localized free K2G molecule diffusion and migration to the surface of TiO_2 with the concentration gradient. Thus, the initial reaction rate for $Fe-TiO_2/AC$ is faster than that for the TiO_2 suspension. Meanwhile, because the Fe ions (dopant) improved the photoactivity of the TiO_2 particles coated on AC, the K2G molecules adsorbed on AC became more easily photodegraded in comparison with those adsorbed on TiO_2/AC. So the synergic effects of Fe ions and AC on TiO_2 largely magnified the photoac-

Figure 7 Photocatalytic degradations for 200 mL K2G solution with catalysts mass of 0.5 g by 0.3%$Fe-TiO_2/AC$ (a); 0.1%$Fe–TiO_2/AC$ (b); 0.5% $Fe-TiO_2/AC$ (c); TiO_2/AC (d); 0.3%$Fe-TiO_2$ (e); P25 (f); TiO_2 (g); the same as curve a, but without UV (h); AC (i). Curves (a−g) were sparged with air in the dark for 200 min before photodegradation in order to eliminate the influence of the adsorbent.
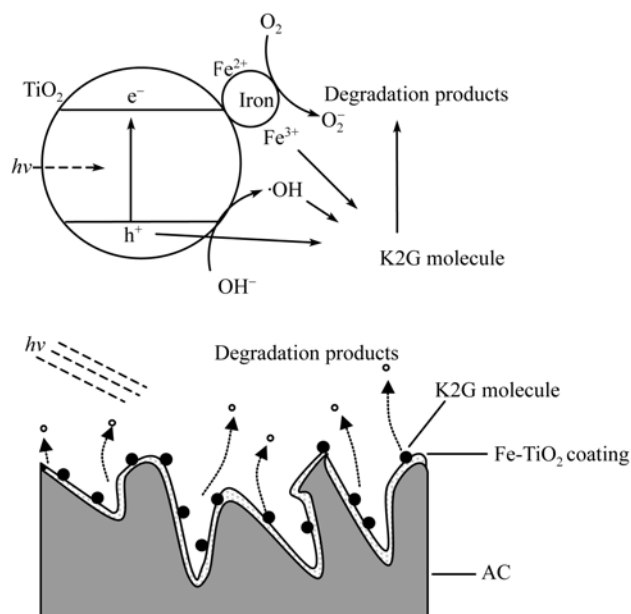

Figure 8 Schematic diagram for the adsorption and photocatalytic degradation of K2G molecules on $Fe-TiO_2/AC$.

tivity of the catalysts. It is indicated that in the course of the photocatalytic reaction, the K2G molecules adsorbed on the surface of AC could easily migrate to the Fe-TiO$_2$ surface due to mass transport differences, and can thus be captured by the photogenerated oxidizing species and finally degraded to give CO$_2$.

4 Conclusions

The Fe-TiO$_2$/AC composite was prepared by an improved sol-gel method using tetrabutylorthotitanate as a precursor. Compared with the agglomeration of pure TiO$_2$, the TiO$_2$ nanoparticles are well dispersed in the AC matrix, of which sizes are decreased with Fe ions doping. The iron species on TiO$_2$ of composite are Fe$_2$O$_3$

and FeO, which do not affect the crystalline structures of TiO$_2$ nanoparticles. Additionally, the fluorescence intensity of composite is affected by AC matrix and iron doping content due to their effects on recombination probability for hole-electron pairs. Compared with TiO$_2$, 0.3% Fe-TiO$_2$, TiO$_2$/AC, 0.5% Fe-TiO$_2$/AC and 0.1% Fe-TiO$_2$/AC, the 0.3% Fe-TiO$_2$/AC shows the highest photoactivity with the complete mineralization of K2G for finite time due to the optimum Fe ions content and AC matrix. Furthermore, the kinetic constant (k) of Fe-TiO$_2$/AC composite is more than the sum of both TiO$_2$/AC and Fe-TiO$_2$ because coexistence of the AC and Fe ions has an enlarging effect on improving the photoactivity of TiO$_2$.

1 Takeda N, Iwata N, Torimoto T, Yoneyama H. Influence of carbon black as an adsorbant used in photocatalyst films on photodegradation behaviors of propyzamide. J Catal, 1998, 177: 240−246

2 Fukahori S, Ichiura H, Kitaoka T, Tanaka H. Capturing of bisphenol a photodecomposition intermediates by composite TiO$_2$-zeolite sheets. Appl Catal B: Environ, 2003, 46: 453−462

3 Alhakimi G, Studnicki L H, Al-Ghazali M. Photocatalytic destruction of potassium hydrogen phthalate using TiO$_2$ and sunlight: Application for the treatment of industrial wastewater. J Photochem Photobiol A: Chem, 2003, 154(2-3): 219−228

4 Shiraishi F, Yamaguchi S, Ohbuchi Y. A rapid treatment of formaldehyde in a highly tight room using a photocatalytic reactor combined with a continuous adsorption and desorption apparatus. Chem Eng Sci, 2003, 58: 929−934

5 Chun H, Yizhong W, Hongxiao T. Destruction of phenol aqueous solution by photocatalysis or direct photolysis. Chemosphere, 2000, 41: 1205−1210

6 Ding Z, Zhu H Y, Lu G Q, Greenfield P F. Photocatalytic properties of titania pillared clays by different drying methods. J Colloid Interface Sci, 1999, 209: 193−199

7 Takeda N, Torimoto T, Sampath S, Kuwabata S, Yoneyama H. Effect of inert supports for titanium dioxide loading on enhancement of photodecomposition rate of gaseous propionaldehyde. J Phys Chem, 1995, 99: 9986−9991

8 Cordero T, Chovelon J M, Duchamp C, Ferronato C, Matos J. Surface nano-aggregation and photocatalytic activity of TiO$_2$ on H-type activated carbons. Appl Catal B: Environ, 2007, 73(3): 227−235

9 Mozia S, Toyoda M, nagaki I M, Tryba B, Morawski A W. Application of carbon-coated TiO$_2$ for decomposition of methylene blue in a photocatalytic membrane reactor. J Hazardous Mater, 2007, 140 (1-2): 369−375

10 Fukahori S, Ichiura H, Kitaoka T, Tanaka H. Photocatalytic decomposition of bisphenol a in water using composite TiO$_2$-zeolite sheets prepared by a papermaking technique. Environ Sci Technol, 2003, 37: 1048−1051

11 Hou H, Miyafuji H, Saka S. Photocatalytic activities and mechanism of the supercritically treated TiO$_2$-activated carbon composites on decomposition of acetaldehyde. J Mater Sci, 2006, 41(24): 8295−8300

12 Wang C C, Lee C K, Lyu M D, Juang L C. Photocatalytic degradation of C.I. Basic Violet 10 using TiO$_2$ catalysts supported by Y zeolite: An investigation of the effects of operational parameters. Dyes Pigm, 2008, 76 (3): 817−824

13 Duminica F D, Maury F, Hausbrand R. Growth of TiO$_2$ thin films by

AP-MOCVD on stainless steel substrates for photocatalytic applications. Surf Coat Tech, 2007, 201(22-23): 9304−9308

14 Cordero T, Duchamp C, Chovelon J M, Ferronato C, Matos J. Influence of L-type activated carbons on photocatalytic activity of TiO$_2$ in 4-chlorophenol photodegradation. J Photochem Photobiol A: Chem, 2007, 191(2-3): 122−131

15 Subramani A K, Byrappa K, Ananda S, Lokanatha K M, Ranganathaiah C, Yoshimura M. Photocatalytic degradation of indigo carmine dye using TiO$_2$ impregnated activated carbon. Bull Mater Sci, 2007, 30(1): 37−41

16 Hou H, Miyafuji H, Kawamoto H, Saka S. Supercritically treated TiO$_2$-activated carbon composites for cleaning ammonia. J Wood Sci, 2006, 52 (6): 533−538

17 Woo S H, Kim W W, Kim S J, Rhee C K. Photocatalytic behaviors of transition metal ion doped TiO$_2$ powder synthesized by mechanical alloying. Mater Sci Eng A, 2007, 448: 151−1154

18 Litter M I, Navío J A. Photocatalytic properties of iron-doped titania semiconductors. J Photochem Photobiol A: Chem, 1996, 98: 171−181

19 Choi W, Termin A, Hoffmann M R. The role of metal ion dopants in quantum-sized TiO$_2$: Correlation between photoreactivity and charge carried recombination dynamics. J Phys Chem, 1994, 98(5): 13669−13679

20 Yang P, Lu C, Hua N P, Du Y K. Titanium dioxide nanoparticles co-doped with Fe^{3+} and Eu^{3+} ions for photocatalysis. Mate Let, 2002, 57: 794−801

21 Sakthivel S, Neppolian B, Shankar M V, Arabindoo B, Palanichamy M, Murugesan V. Solar photocatalytic degradation of Azo Dye: Comparison of photacatalytic efficiency of ZnO and TiO$_2$. Energy Mater Sol Cell, 2003, (77): 65−71

22 Yamashita H, Harada M, Misaka J, Takeuchi M, Ikeue K, Anpo M. Degradation of propanol diluted in water under visible light irradiation using metal ion-implanted titanium dioxide photocatalysts. J Photochem Photobiol A: Chem, 2002, 148: 257−261

23 Yu J G, Zhao X J. Effect of surface treatment on the photocatalytic activity and hydrophilic property of the sol-gel derived TiO$_2$ thin films. Mater Res Bull, 2000, 36: 97−107

24 Liu B J, Torimoto T, Yoneyama H. Photocatalytic reduction of CO$_2$ using surface-modified CdS photocatalysts in organic solvents. J Photochem Photobiol A: Chem, 1998, 113: 93−97

25 Inoue H, Moriwaki H, Maeda K, Yoneyama H. Photoreduction of carbon dioxide using chalcogenide semiconductor microcrystals. J Photochem Photobiol A: Chem, 1995, 86: 191−196

LI YouJi et al. Sci China Ser B-Chem | Aug. 2009 | vol. 52 | no. 8 | **1113-1119**

1119